Influence of Cracking on Moisture Uptake in Strain-Hardening Cementitious Composites

Savija, Branko; Lukovic, Mladena; Schlangen, Erik

DOI
10.1061/(ASCE)NM.2153-5477.0000114

Publication date
2016

Document Version
Accepted author manuscript

Published in
Journal of Nanomechanics and Micromechanics

Citation (APA)
Savija, B., Lukovic, M., & Schlangen, E. (2016). Influence of Cracking on Moisture Uptake in Strain-Hardening Cementitious Composites. *Journal of Nanomechanics and Micromechanics*, 1-8. Article 04016010. https://doi.org/10.1061/(ASCE)NM.2153-5477.0000114

INFLUENCE OF CRACKING ON MOISTURE UPTAKE IN STRAIN HARDENING CEMENTITIOUS COMPOSITES

Branko Šavija[1*], PhD, Mladena Luković[2], PhD, and Erik Schlangen[3], PhD

Abstract

Strain hardening cementitious composites (SHCC) are a class of cement based materials which show strain hardening behaviour in tension. This is achieved by multiple microcracking, which results in a tightly spaced crack pattern with relatively small crack widths (50-80 micrometers (μm), in general) and high strain capacity (up to 4-5%). Due to their ductile behaviour and tight crack widths, SHCCs are commonly used for concrete repair applications. However, due to the tight crack width and crack spacing, moisture uptake by capillary suction can take place very fast. This could result in rapid access of deleterious substances, such as chloride ions, resulting in corrosion initiation. In this study, X-ray tomography is used for monitoring and quantification of water uptake in SHCC. Specimens were first loaded to different strain levels in uniaxial tension. Then, they were subjected to a capillary suction test. The performed test was subsequently modelled using a lattice model.

Keywords: SHCC, composite, durability, X-ray attenuation, modelling

1-Post doctoral researcher, Microlab, Faculty of Civil Engineering and Geosciences, Delft University of Technology, Delft, The Netherlands

2- Post doctoral researcher, Concrete Structures Group, Faculty of Civil Engineering and Geosciences, Delft University of Technology, Delft, The Netherlands; Formerly a PhD candidate, Microlab, Faculty of Civil Engineering and Geosciences, Delft University of Technology, Delft, The Netherlands

3- Professor of Experimental Micromechanics, Microlab, Faculty of Civil Engineering and Geosciences, Delft University of Technology, Delft, The Netherlands

*-corresponding author, e-mail: b.savija@tudelft.nl

Revised manuscript submitted to Journal of Nanomechanics and Micromechanics

INTRODUCTION

Corrosion of steel reinforcement is a well-recognized deterioration mechanism of reinforced concrete structures. The steel reinforcement is, under normal circumstances, protected by the high pH of the alkaline concrete. If this protection is lost, which could happen either due to carbonation or chloride ingress, active corrosion of the reinforcement will take place (Bertolini, et al., 2013). Corrosion of steel reinforcement has several important consequences: it causes cracking and spalling of the concrete cover, thereby speeding up the deterioration (Šavija, et al., 2013); it reduces the effective area of reinforcement, thereby lowering its load-bearing capacity (Yoon, et al., 2000); and affects the bond between steel and concrete (Lee, et al., 2002, Grassl and Davies, 2011). Therefore, it is of critical importance to protect the reinforcement from corrosion initiation.

Consequently, the durability of reinforced concrete depends on the quality and on the integrity of the protective cover. This is somewhat problematic, as reinforced concrete structures are prone to cracking, due to e.g. mechanical loading or restrained shrinkage. Although most cracks do not present risks for structural safety and reliability of a structure, they can be fast routes for moisture carrying corrosive substances such as chloride ions and carbon dioxide (CO_2) (De Schutter, 1999, Šavija, 2014). Therefore, it is necessary to limit the extent of cracking in reinforced concrete structures. Due to the quasi-brittle behaviour of plain concrete (Van Mier, 2012), this is commonly achieved by increasing the amount of reinforcing steel. In recent years, a different approach has been developed: namely, creating cement-based materials with strain-hardening properties.

SHCC (strain-hardening cementitious composite) is a class of ultra-ductile cement based materials which exhibit hardening under tensile loading (Li, et al., 2001). This is achieved by multiple microcracking, which results in a tightly spaced crack pattern with relatively small crack widths (50-80μm, in general) and high strain capacity (up to 4-5%) (Li, 2003). It is, therefore, believed that SHCCs should have higher durability compared to concrete (Chandra Paul and van Zijl, 2014, Šavija, et al., 2015). This notion was recently questioned by (Wang, et al., 2014), who found that SHCC under

strain imbibes water very rapidly by capillary action. Therefore, the issue of water uptake in crack SHCC needs to be further investigated.

In this study, moisture uptake in cracked SHCC is monitored non-destructively by using the X-ray absorption technique. First, SHCC specimens are loaded in uniaxial tension. After unloading, they are subjected to water penetration in a moisture uptake test. This is monitored by X-ray absorption. Finally, moisture uptake in cracked SHCC is simulated using an experimentally-informed modelling procedure within the lattice modelling framework.

MATERIALS AND METHODS

Materials and specimen preparation

Materials used in the SHCC mixture were Ordinary Portland Cement (CEM I 42.5N), limestone powder, blast furnace slag (BFS), water, superplasticizer, and polyvinyl alcohol (PVA) fibres. Mix proportions are given in Table 1 (Zhou, et al., 2010). Mixing procedure was as follows: first, solid materials (powder plus the PVA fibres) were mixed for 2.5 minutes at low speed; then, water (together with the superplasticizer) was added, and mixed for an additional minute at low speed; finally, the mixing procedure was continued for additional 4 minutes at high mixing speed. The material was cast into PVC moulds and compacted using a vibrating table.

Table 1. SHCC mix proportions (weight ratio)

Ingredient	Quantity
CEM I 42.5 N	0.6
Limestone powder	2
Blastfurnace slag	1.4
Water/powder ratio	0.26
Superplasticizer	0.02
PVA fiber (by volume, %)	2

In total, five coupon specimens were then cast for uniaxial tension tests (Figure 1). The specimens were sealed, demolded after one day, and cured in a fog room at 20°C and 95% RH (relative humidity) for 28 days. Afterwards, the specimens were kept in laboratory conditions until testing (around 20°C

and 50% RH). At the age of 40 days, they were subjected to uniaxial tension (figure 2). Afterwards, slices (about 3cm wide) were cut from the middle portion of each specimen to be subjected to the moisture-uptake test. In general, areas with visible cracks were selected for slicing. Prior to testing, these slices were dried overnight in an oven at 35°C. Samples dried in that way were subjected to moisture uptake by capillary suction, while X-ray absorption measurements were performed. Note that the drying procedure (i.e. the initial moisture content in the specimen) has a marked effect on the water uptake (Rucker-Gramm and Beddoe, 2010), and some authors suggest drying at 105°C in order to remove all evaporable water (Hall, 1989). In order to avoid possible microcracking, a lower preconditioning temperature was used here. Specimens were wrapped in a self-adhesive aluminium tape to ensure a one-dimensional moisture ingress.

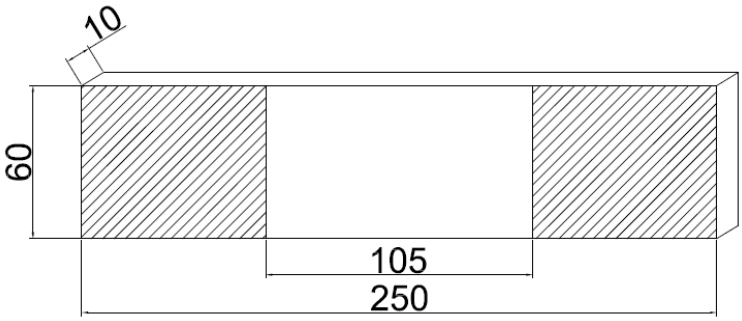

Figure 1. Geometry of an SHCC coupon specimen (Hatched areas were glued and clamped, leaving the middle free to deform). (Sizes are in mm)

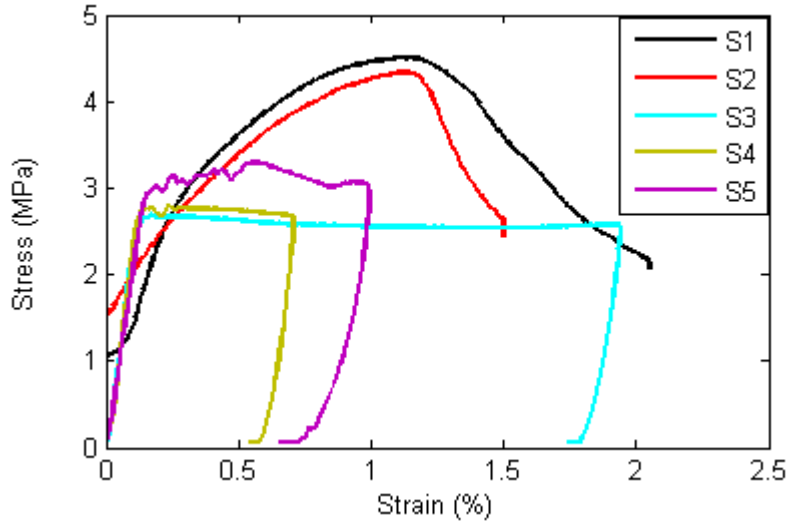

Figure 2. Stress-strain diagrams of the tested SHCC specimens.

X-Ray attenuation technique

The specimens were tested in a Phoenix Nanotom X-ray system (Computed Tomography scanner-CT) for measuring the moisture uptake. CT scans are 3D maps of X-ray absorption in the material (Herman, 2009). In CT scanning, multiple X-ray images of a specimen are taken at different angles, and the 3D image is then reconstructed. In this research, however, X-ray images were taken only perpendicular to the specimen. The resulting images are spatial distributions of linear attenuation coefficients, expressed as grey scale values (*GSV*). In general, the attenuation of monochromatic X-rays can be described by Beer-Lambert law (Roels and Carmeliet, 2006, Michel, et al., 2011, Luković and Ye, 2016):

$I = I_0 e^{-\mu t}$	(1)

where μ is the attenuation coefficient, t the specimen thickness, and I_0 the incident intensity. In the X-ray image obtained by the Nanotom X-ray system, the intensity I is expressed in the form of grey scale values. The change in *GSV* of each pixel can, in the presented setup, be correlated with the change in moisture content of a porous material (such as SHCC) by taking advantage of the following: in a dry porous material, X-rays get attenuated by the dry material *only*; if the pores are instead filled with water, X-rays will be attenuated by the dry material plus water (Figure 3). Thanks to this, and by knowing the attenuation coefficient of pure water, it is possible to calculate the amount of (additional) water in a porous material from changes in *GSV*. Due to variations of beam intensity, the measured attenuation coefficient of water could vary slightly between individual experiments. It was, therefore, measured prior to each experiment by utilizing a plastic container of a known width and comparing the *GSV* of it with and without added water (see figure 4). Further details about the application of the technique to moisture exchange in porous materials can be found in (Luković, 2016, Luković and Ye, 2016).

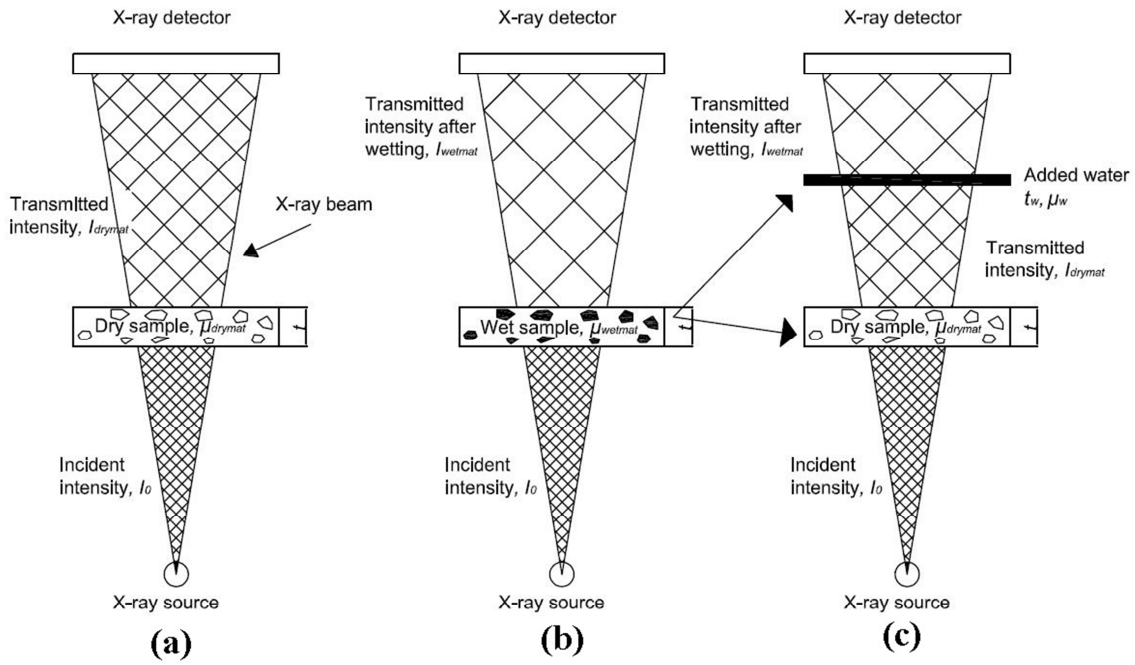

Figure 3. Use of X-ray measurements on determination of moisture content in porous materials. The moisture distribution is obtained by logarithmically subtracting an image of the dry sample (a) from an image of the wet sample (b). Note that the effect of add

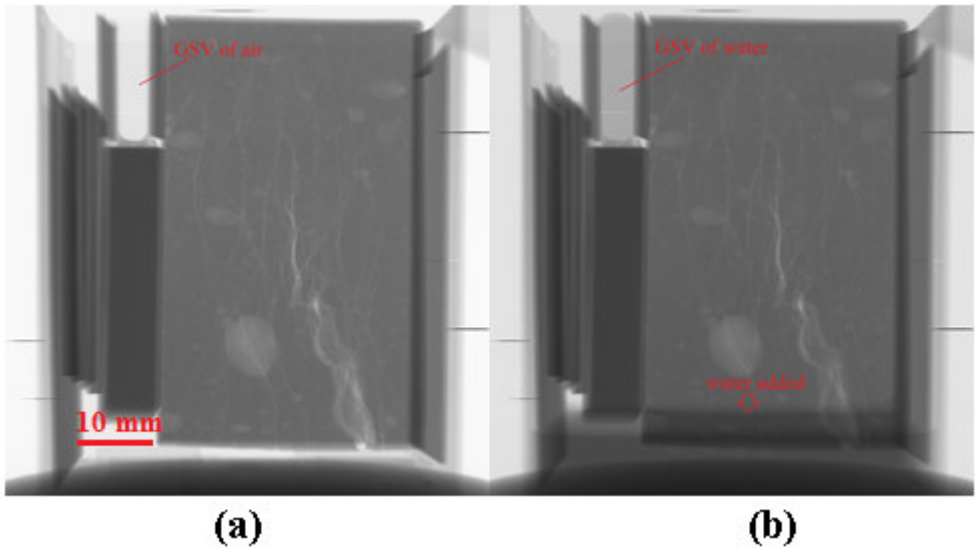

Figure 4. Examples of a reference image (a) and image taken during the experiment (b)

As described earlier, pre-conditioned specimens were placed in the chamber of the CT scanner (Figure 5). Water was then added, and images were taken during its uptake. The achieved spatial resolution was around 30μm, which limits the size of cracks which could be observed, as explained later.

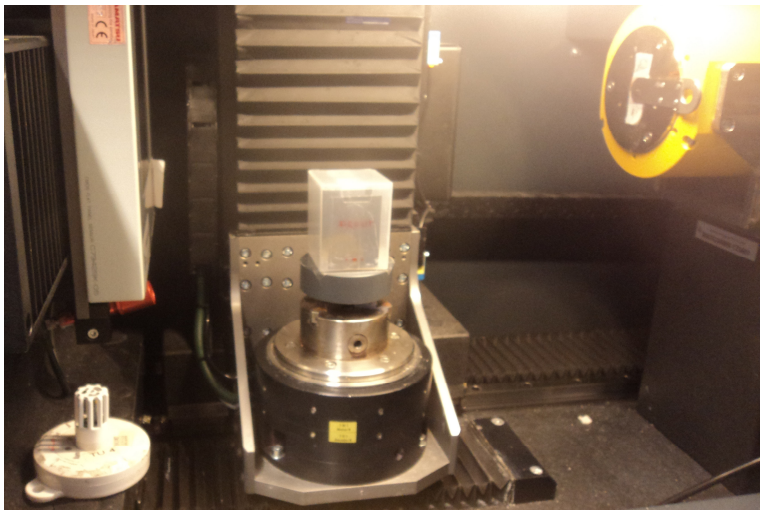

Figure 5. A specimen inside of the chamber of the CT scanner.

Lattice modelling

Lattice models have been used in the past to simulate fracture of concrete and other heterogeneous materials (Schlangen and Van Mier, 1992, Bolander and Saito, 1998, Vasic, et al., 2005, Šavija, et al., 2016). Fracture in fibre reinforced composites can also be simulated (Bolander and Saito, 1997, Luković, et al., 2014, Montero-Chacón, et al., 2015). Furthermore, the lattice modelling concept has recently been extended on simulating mass transport processes in sound and cracked porous materials (Bolander and Berton, 2004, Grassl, 2009, Grassl, et al., 2010, Wang and Ueda, 2011, Šavija, et al., 2013, Abyaneh, et al., 2014). Such models are nowadays able to simulate the coupling of mechanical and transport processes. In this work, only moisture uptake in cracked SHCC is simulated.

In the model used herein, SHCC material is discretized as a set of one-dimensional linear ("pipe") elements through which moisture flow takes place. Governing equation for moisture transport has the following form:

$$\frac{\partial \theta}{\partial t} = \frac{\partial}{\partial x}\left(D(\theta)\frac{\partial \theta}{\partial x} \right) \quad (2)$$

where $D(\theta)$ is the hydraulic diffusivity and θ the moisture content. (Hall, 1989) showed that, mathematically speaking, it is possible to re-express the unsaturated flow equation as a diffusion equation in a mathematical sense (equation 1). It needs to be emphasized that, even though equation 2 is mathematically a diffusion-type equation, the governing transport mechanism in this case is

capillary absorption, and not diffusion. This is justifiable when gravitational effects on the flow are small (Hall, 1989), which is mostly the case when dealing with transport in porous building materials.

If equation 2 is discretized using the standard Galerkin procedure, the following set of equations results (Lewis, et al., 1996):

$$M\frac{d\theta}{dt}+K\theta=f \tag{3}$$

where M is the element mass matrix, K element diffusion matrix, and f the element forcing vector. Vector of unknown quantities, θ, is the vector of moisture contents in nodes of a lattice element. Elemental matrices have the following form:

$$M=\frac{Al}{6\omega}\begin{bmatrix}2 & 1\\ 1 & 2\end{bmatrix} \tag{4}$$

$$K=\frac{D(\theta)A}{l}\begin{bmatrix}1 & -1\\ -1 & 1\end{bmatrix} \tag{5}$$

$$f=\begin{bmatrix}-q_i A\\ -q_j A\end{bmatrix} \tag{6}$$

Here, l is the element length, A the element cross-sectional area. If a random lattice is used (as was done in previous studies by the authors (Šavija, et al., 2013, Šavija, et al., 2014)), cross-sectional areas of individual lattice elements are assigned using the so-called Voronoi scaling method (Yip, et al., 2005). ω is a correction factor equal to 1 for 1D, 2 for 2D, and 3 for 3D analyses (Bolander and Berton, 2004). Note that, in this work, a regular square lattice is used (see section 2.4), so all elements have the same cross-sectional area.

Equation (3) can be discretized in time using the Crank-Nicholson procedure (Lewis, et al., 1996) (assuming that no flux boundary conditions are applied, i.e. *f=0*):

$$(M+\frac{1}{2}\Delta t\cdot K)\theta^{n}=(M-\frac{1}{2}\Delta t\cdot K)\theta^{n-1} \tag{7}$$

Equation 7 can be solved for each discrete time step Δt. It needs to be emphasized that hydraulic diffusivity D and, therefore, diffusion matrix K is dependent on the moisture content θ. This makes equation 2 non-linear. To avoid solving the non-linear set of equations using an iterative procedure (such as the Newton-Raphson method), the diffusion matrix K in each step is calculated using the moisture content θ from the previous step. The error which occurs due to this simplification can be considered negligible if small time steps Δt are used, while it significantly shortens the calculation time.

Experimentally-informed modelling procedure

In principle, it is possible to simulate fracture in SHCC using a lattice-type model (Kang, et al., 2014, Luković, et al., 2014). These models are capable of reproducing global strain-hardening behaviour and local multiple cracking in such materials. However, the rate of moisture uptake is highly dependent on local pores and microcracks. Since it is normally not possible to capture exact location and geometry of cracks in a uniaxial test of SHCC using numerical modelling, in this work a different approach is taken, as explained below.

In the preliminary study (Šavija, et al., 2015), X-ray images of a cracked specimen (such as those shown in Figure 4) were thresholded in order to isolate cracks and pores. Such a thresholded image was used to create a lattice mesh, which was subsequently used to simulate moisture uptake. In this preliminary study, threshloding was performed using the following procedure: First cracks and pores were isolated based on their *GSV* (taking advantage of the fact that cracks, pores, and voids are much brighter compared to the bulk material). The thresholding point was selected using trial-and-error, which can be considered as one of the limitations of the current approach, unlike well-established techniques for pore separation in back scatter electron images (Wong, et al., 2006). Then, each large crack was isolated and individual cracks skeletonized. Finally, individual crack images were combined to provide a base image on which the lattice mesh was projected. However, due to limitations in spatial resolution (30μm in this case), only cracks larger then this were taken into account in the simulation. This resulted in an underestimation of moisture uptake compared to the experimental observations (see figure 6). As a consequence, an improved procedure is proposed here.

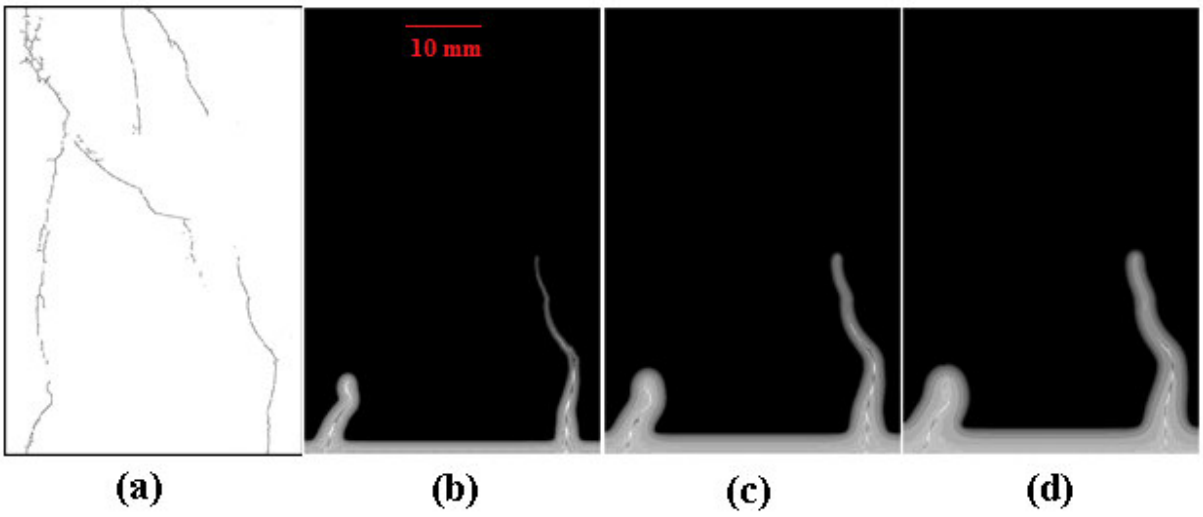

Figure 6. Simulation results from the preliminary study (a) lattice mesh; moisture profiles after 10 (b), 20 (c), and 30 min (d). Colour legend is the same as in figure 9, while experimental results are shown in figure 10.

A significant local increase in moisture uptake is a clear indicator of existence of a crack. Therefore, instead of directly using X-ray images, a processed image showing moisture distribution was exploited as a basis to determine the “real” distribution of cracks. thresholded, and cracks highlighted. The fact that “wet” part of the specimen is darker than the “dry” part of the specimen (Figure 7 left) was used as a basis for the thresholding: using trial and error for selecting the thresholding point, the wet areas were isolated. Then, lines representing cracks were drawn by hand following these areas of increased moisture uptake (Figure 7 middle). In the end, such processed and simplified image was used to create a lattice mesh (Figure 7 right). Midpoints of each pixel were connected with the neighbouring pixels to create a (square) lattice mesh. Two types of lattice elements are created, depending on the "state" of their end nodes (see Figure 8): "matrix" elements and "crack" elements. Note that it is not possible to obtain exact information about the width of individual cracks with this procedure. This is the reason why all cracks were assumed to have the same transport properties.

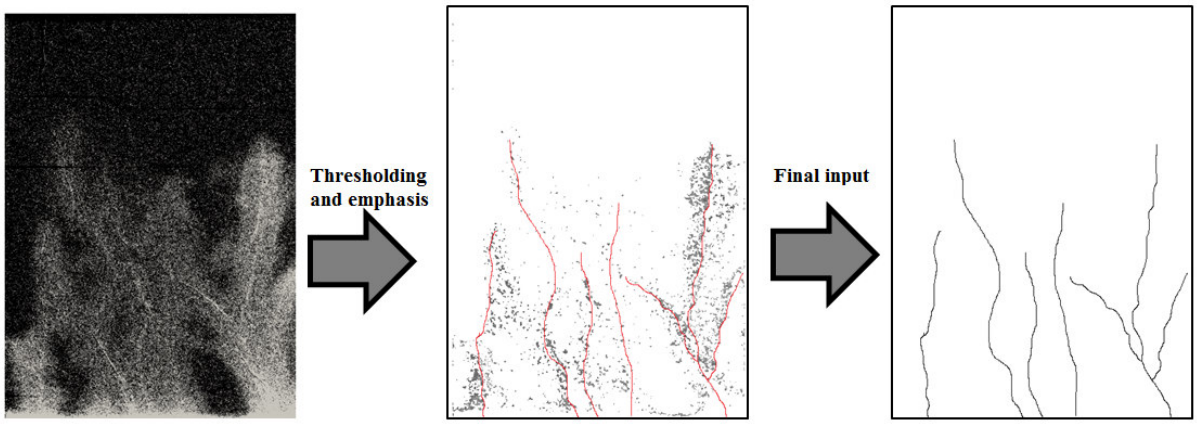

Figure 7. Creating input for numerical simulations.

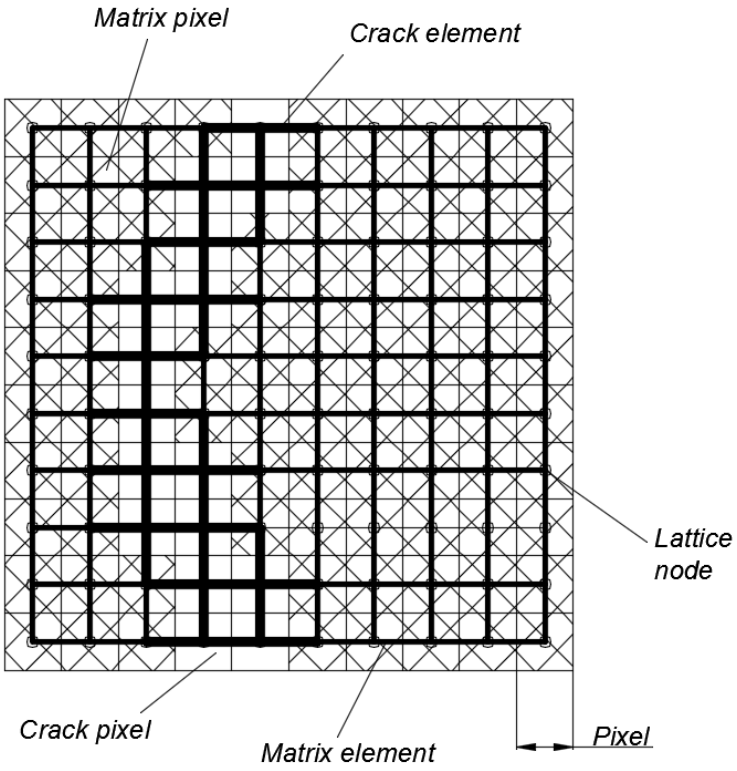

Figure 8. Creating a lattice mesh from an image.

RESULTS AND DISCUSSION

Experimental results

Water penetration into SHCC specimens (prepared and cracked as described in section 2) was visualized by means of X-ray absorption. In this section, moisture uptake in specimens 1, 3, 4, and 5 is examined. These specimens were loaded in uniaxial tension to 2%, 2%, 0.75%, and 1.0%,respectively. The loading induced different extents of microcracking in the specimens. As stated previously,

sections of about 3cm width were cut from each of the samples, dried, and subjected to moisture uptake. Note that these sections were selected to sample as many cracks as possible (based on visual observation). In the top row of figure 9, cracks in each of the used slices (captured by X-ray absorption) are highlighted for visibility. Note that specimen 2 was used for numerical simulations, and its results are shown in the following section.

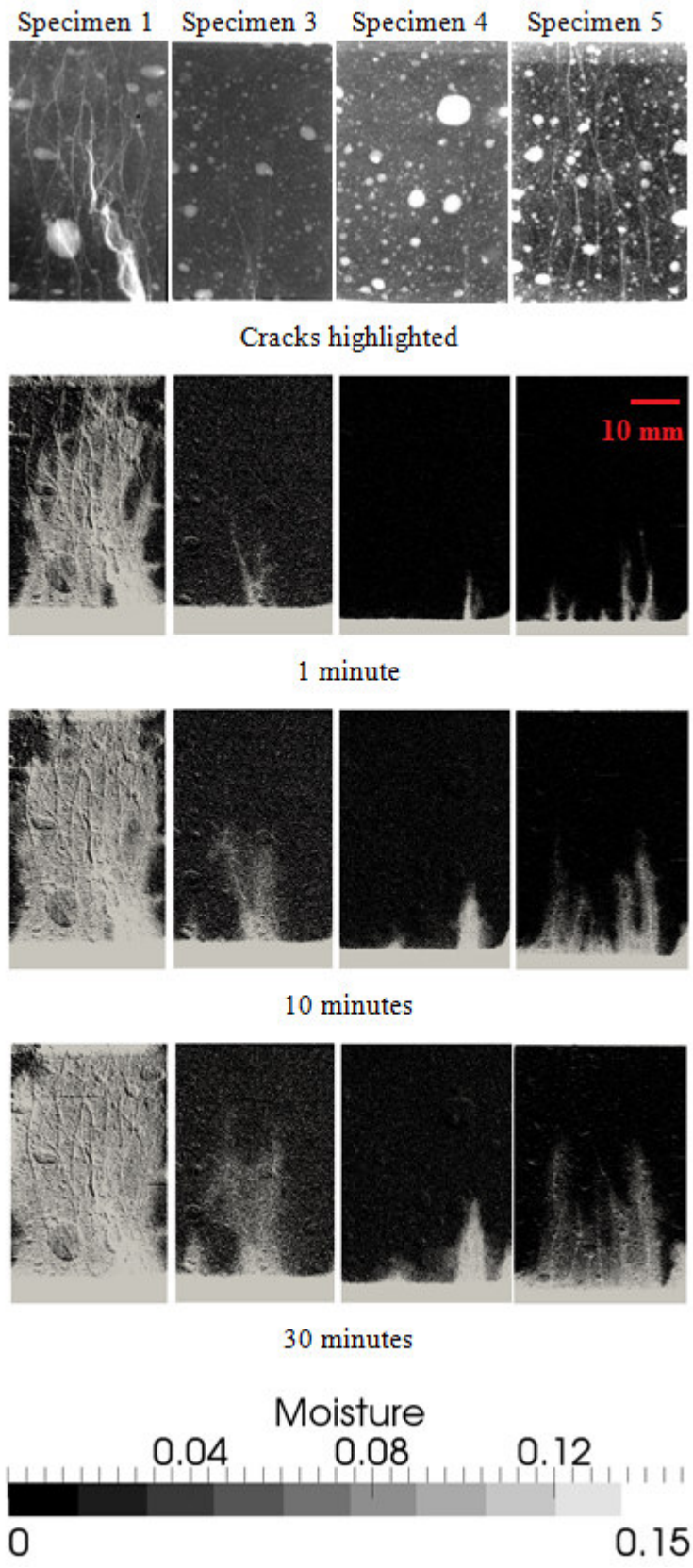

Figure 9. Experimental results of moisture uptake in specimens 1, 3, 4, and 5.

Specimen 1 shows a large number of observable cracks, with one major crack accompanied by multiple narrow cracks (Figure 9). Already after 1 minute of water uptake, the water front reaches the top of the specimen. After 10 minutes, the moisture front broadens, as more and more cracks are filled with water. After 30 minutes, the water front covers more or less the whole specimen.

Specimen 3 shows only minor cracks (Figure 9). These cracks are rapidly filled with water after 1 minute, with the moisture front becoming deeper and wider after 10 and 30 minutes. It can be noted that, although specimens 1 and 3 were loaded to similar levels (2 % strain, see figure 2), the slices used for moisture uptake measurements showed markedly different extents of cracking. This is probably a consequence of the experimental setup used for the uniaxial tensile test: in the test, supports were free to rotate, thereby allowing that bending stresses can arise due to possible small eccentricities. This could have caused non-uniform stress distributions in some of the specimens, which could have resulted in localization of cracks. Consequently, the moisture uptake is markedly different between these two specimens, being significantly higher in specimen 1 than in specimen 3. Moisture uptake in cracks is a local phenomenon, depending not on the global strain and cracking behaviour, but on the existence of (local) defects and cracks. This is the main reason why experiments are used as input for moisture uptake simulations, and not mechanical simulations, since they are (still) unable to provide such fine level of detail (Luković, et al., 2014). In the work of (Wang, et al., 2014) it was suggested to prescribe a strain limit for SHCC based on durability considerations. Based on the findings presented herein, it seems that a conservative limit strain should be selected in this case due to the high scatter in individual crack widths and, thus, in the resulting moisture uptake.

Specimen 4, which was loaded to 0.75% strain, shows only one visible narrow crack (Figure 9). This crack is filled with moisture rapidly (already after 1 minute), with the moisture front becoming a bit deeper, but significantly wider, after 10 and 30 minutes. This resembles the behaviour of regular concrete, where the (single) crack gets filled almost instantaneously by capillary action, and then the water migrates from the crack into the surrounding concrete (Zhang, et al., 2010).

Specimen 5 (loaded to 1% strain) shows a large number of narrow cracks (Figure 9). However, from moisture profiles observed in this specimen, it seems that these cracks are not continuous across the height of the specimen. As a consequence, only a small portion of the visible cracks are rapidly filled with water (after 1 min). After 10 minutes, the water front is deeper and somewhat wider, while after 30 minutes it goes past one half of the specimen height. Still, even after 30 minutes, the water front does not reach the top of the specimen. This is in clear contrast to specimen 1. It is probable that, since specimen 1 was loaded more than specimen 3 (2% vs. 1% strain, respectively), more cracks became interconnected in that case, creating a continuous route for rapid moisture ingress.

From the experiments performed, it can be inferred that the small cracks which form in SHCC significantly promote capillary moisture uptake compared to uncracked parts of the material. In practice, this water could contain for example chloride ions which would cause fast initiation of reinforcement corrosion, and therefore significantly shorten the service life of the structure in question (Blagojević, 2016). It should be noted that this fact has significant practical implications. In research and engineering practice it is commonly assumed that structures with smaller cracks are more durable compared to those with wide cracks. This is probably true for saturated structures, where ionic diffusion of chlorides is the leading transport mechanism(Ismail, et al., 2008, Šavija, 2014). However, for unsaturated structures, the issue could be more complex. When the surrounding material is dry, a crack could be acting as a capillary. Considering simple capillary action it can be concluded that, indeed, liquid rise is inversely proportional to the radius of the capillary (Batchelor, 2000). In unsaturated cases, therefore, salt water could penetrate the fine cracks in SHCC very fast and initiate corrosion. Therefore, in spite of its superior mechanical performance in terms of strain capacity (compared to conventional concrete), SHCC may be more vulnerable for certain deterioration mechanisms when unsaturated. In that respect, it can be considered that application of water repellent treatments at the SHCC surface, as proposed by (Wang, et al., 2014), is a good option in some environments. With respect to chloride ingress and reinforcement corrosion, it should be pointed out here , however, that recent findings suggest that the damage at the steel/concrete interface is much more significant compared to the surface crack width in terms of both initiation and propagation of

reinforcement corrosion (Michel, et al., 2013, Šavija, et al., 2014, Blagojević, 2016): it is quite probable that this damage is lower in SHCC compared to conventional concrete. This should be a subject of further study.

Modelling results

In this section, experiment on specimen 2, which was loaded up to a strain of around 1.5%, is simulated using the approach described in section 2. The non-linear relationship between the hydraulic diffusivity D and the moisture content θ can be described as:

$$D(\theta) = D_0 e^{n\theta} \quad (8)$$

where D_0 and n are empirical fitting parameters. These parameters can be obtained from moisture profiles measured on an uncracked sample using the fitting procedure described by (Pel, 1995), which uses Boltzmann transformations of measurement curves to obtain the fitting parameters . For the presented case, these parameters were calculated as: $D_0 = 0.197$ and $n = 50.067$. These parameters were obtained using measurements of water uptake in an additional uncracked sample. Alternatively, a simpler procedure proposed by (Wang and Ueda, 2011) could be used to obtain a rough estimate of the fitting parameters.

The lattice mesh is created using the procedure shown in figure 7. Crack elements in the lattice are ascribed an additional multiplication factor equal to 5000 in equation 8 to account for the increase in their hydraulic diffusivity. At the bottom of the mesh, a Dirichlet boundary condition is imposed.

The comparison between the experimental results and the simulation is given in figure 10. Whereas in the initial study (Šavija, et al., 2015), where cracks were directly thresholded from X-ray images, the moisture uptake was grossly underestimated (see figure 6), the improved procedure provides better results. After 10 minutes, several sharp moisture fronts form around the cracks. After 20 minutes, these fronts are significantly wider and less sharp. After 30 minutes, these fronts start to merge in the lateral direction. The lattice model is able to replicate such behaviour and the transition from a very sharp to a wider front with elapsed exposure. The proposed procedure for creating the lattice can circumvent the limited spatial resolution of the X-ray scan.

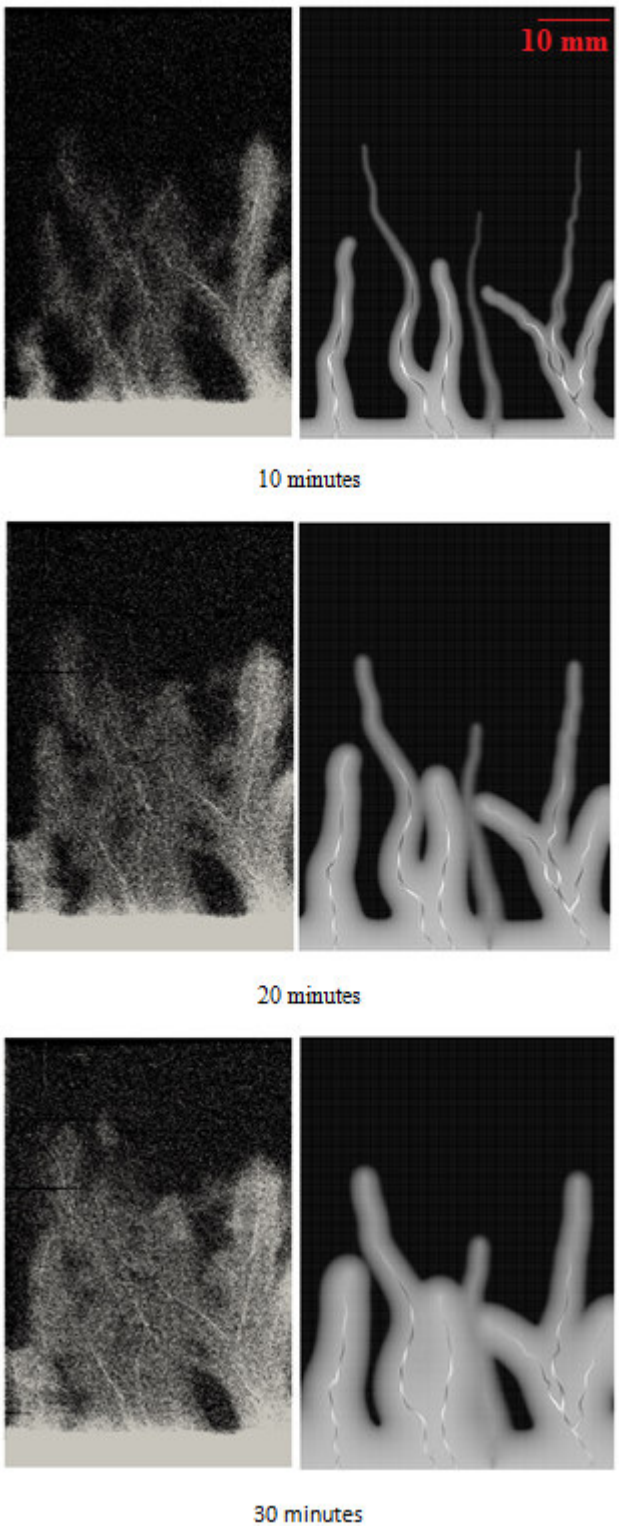

Figure 10. Comparison of experimental and simulation results for moisture uptake in specimen 2. Colour legend is the same as in figure 9.

Even though it is observed that the model reflects the experimental behaviour quite well, it does have certain drawbacks. First, the procedure for thresholding of cracks which is employed to create the mesh is quite subjective and operator dependent: although steps which are proposed can be easily

followed, the thresholding point was selected manually. This issue is not trivial, since X-ray attenuation essentially samples a three-dimensional body, which is projected in a two-dimensional image: each pixel is, therefore, an average of all pixels transversed by the same X-ray. This is, of course, a simplification, since pores and cracks are three-dimensional even in a 10mm thick specimen as the one used herein. The second major assumption that was that the transport properties of all cracks are the same, independent on their crack width: in reality, transport properties of cracks are dependent on their width. In order to improve this, it would be needed to retain information of crack widths from the images. For the initial procedure (Šavija, et al., 2015), this was possible but limited by the spatial resolution of X-ray images: for the improved procedure used herein, this is not possible at the moment. Finally, the ideal situation would be to use the mechanical simulation instead of experiments as input for the transport simulation. For this, the level of detail in mechanical simulations need to be increased. One possible option would be development of multi-scale mechanical models for simulating fracture in fibre reinforced cementitious composites within the lattice modelling framework.

CONCLUSIONS

In this paper, monitoring of moisture uptake in strained (cracked) SHCC specimens using X-ray attenuation technique is presented. Furthermore, an experimentally-informed modelling procedure for modelling moisture uptake in cracked SHCC was proposed, within the lattice modelling framework. Based on the results presented in this work, several conclusions can be drawn:

- X-ray absorption technique is a good way of monitoring moisture movement in (cracked) SHCC with a high spatial resolution.
- Water uptake by capillary action is very rapid in cracked SHCC due to its multiple cracking ability. Already after 1 minute, cracks are filled with water, while at later times water migrates laterally from the cracks into the material. Depending on the crack geometry, the moisture front can go all the way through the specimen. This could possibly have a negative effect on

durability of steel reinforced SHCC, because chloride ions could reach the rebars very fast, thus initiating corrosion. This is in line with a previous study of (Wang, et al., 2014).

- A direct relation between the applied stress and the moisture ingress was not found. Instead, the amount of water uptake was related to the number and connectivity of cracks. This was probably related to the fact that, out of each specimen, only a small piece was used for moisture uptake measurements.
- It was possible to overcome issues of spatial resolution of the X-ray images with an innovative modelling procedure. Simulation results show good agreement with the experiment.

ACKNOWLEDGEMENTS

B.Š. would like to acknowledge the financial support of European Union Seventh Framework Programme (FP7/2007-2013) under grant agreement no 309451 (HEALCON). The authors would also like to acknowledge the help of Mr. Gerrit Nagtegaal with the mechanical testing and Mr. Arjan Thijssen with X-ray absorption experiments.

REFERENCES:

Abyaneh, S. D., Wong, H., and Buenfeld, N. (2014). "Computational investigation of capillary absorption in concrete using a three-dimensional mesoscale approach." *Computational Materials Science*, 87, 54-64.

Batchelor, G. K. (2000). *An introduction to fluid dynamics*, Cambridge university press.

Bertolini, L., Elsener, B., Pedeferri, P., Redaelli, E., and Polder, R. B. (2013). *Corrosion of steel in concrete: prevention, diagnosis, repair*, John Wiley & Sons.

Blagojević, A. (2016). "The Influence of Cracks on the Durability and Service Life of Reinforced Concrete Structures in relation to Chloride-Induced Corrosion: A Look from a Different Perspective." PhD thesis, Delft University of Technology, Delft, Netherlands.

Bolander, J., and Saito, S. (1997). "Discrete modeling of short-fiber reinforcement in cementitious composites." *Advanced Cement Based Materials*, 6(3), 76-86.

Bolander, J., and Saito, S. (1998). "Fracture analyses using spring networks with random geometry." *Engineering Fracture Mechanics*, 61(5), 569-591.

Bolander, J. E., and Berton, S. (2004). "Simulation of shrinkage induced cracking in cement composite overlays." *Cement and Concrete Composites*, 26(7), 861-871.

Chandra Paul, S., and van Zijl, G. P. (2014). "Crack Formation and Chloride Induced Corrosion in Reinforced Strain Hardening Cement-Based Composite (R/SHCC)." *Journal of Advanced Concrete Technology*, 12(9), 340-351.

De Schutter, G. (1999). "Quantification of the influence of cracks in concrete structures on carbonation and chloride penetration." *Magazine of Concrete Research*, 51(6), 427-435.

Grassl, P. (2009). "A lattice approach to model flow in cracked concrete." *Cement and Concrete Composites*, 31(7), 454-460.

Grassl, P., and Davies, T. (2011). "Lattice modelling of corrosion induced cracking and bond in reinforced concrete." *Cement and Concrete Composites*, 33(9), 918-924.

Grassl, P., Wong, H. S., and Buenfeld, N. R. (2010). "Influence of aggregate size and volume fraction on shrinkage induced micro-cracking of concrete and mortar." *Cement and Concrete Research*, 40(1), 85-93.

Hall, C. (1989). "Water sorptivity of mortars and concretes: a review." *Magazine of Concrete Research*, 41(147), 51-61.

Herman, G. T. (2009). *Fundamentals of computerized tomography: image reconstruction from projections*, Springer Science & Business Media.

Ismail, M., Toumi, A., François, R., and Gagné, R. (2008). "Effect of crack opening on the local diffusion of chloride in cracked mortar samples." *Cement and Concrete Research*, 38(8), 1106-1111.

Kang, J., Kim, K., Lim, Y. M., and Bolander, J. E. (2014). "Modeling of fiber-reinforced cement composites: discrete representation of fiber pullout." *International Journal of Solids and Structures*, 51(10), 1970-1979.

Lee, H.-S., Noguchi, T., and Tomosawa, F. (2002). "Evaluation of the bond properties between concrete and reinforcement as a function of the degree of reinforcement corrosion." *Cement and Concrete Research*, 32(8), 1313-1318.

Lewis, R. W., Morgan, K., Thomas, H., and Seetharamu, K. (1996). *The finite element method in heat transfer analysis*, John Wiley & Sons.

Li, V. C. (2003). "On engineered cementitious composites (ECC)." *Journal of Advanced Concrete Technology*, 1(3), 215-230.

Li, V. C., Wang, S., and Wu, C. (2001). "Tensile strain-hardening behavior of polyvinyl alcohol engineered cementitious composite (PVA-ECC)." *ACI Materials Journal*, 98(6), 483-492.

Luković, M. (2016). "Influence of interface and strain hardening cementitious composite (SHCC) properties on the performance of concrete repairs." PhD thesis, Delft University of Technology, Delft, Netherlands.

Luković, M., Dong, H., Šavija, B., Schlangen, E., Ye, G., and van Breugel, K. (2014). "Tailoring strain-hardening cementitious composite repair systems through numerical experimentation." *Cement and Concrete Composites*, 53, 200-213.

Luković, M., and Ye, G. (2016). "Effect of Moisture Exchange on Interface Formation in the Repair System Studied by X-ray Absorption." *Materials*, 9(1), 2.

Michel, A., Pease, B. J., Geiker, M. R., Stang, H., and Olesen, J. F. (2011). "Monitoring reinforcement corrosion and corrosion-induced cracking using non-destructive x-ray attenuation measurements." *Cement and Concrete Research*, 41(11), 1085-1094.

Michel, A., Solgaard, A. O. S., Pease, B. J., Geiker, M. R., Stang, H., and Olesen, J. F. (2013). "Experimental investigation of the relation between damage at the concrete-steel interface and initiation of reinforcement corrosion in plain and fibre reinforced concrete." *Corrosion Science*, 77, 308-321.

Montero-Chacón, F., Schlangen, E., Cifuentes, H., and Medina, F. (2015). "A numerical approach for the design of multiscale fibre-reinforced cementitious composites." *Philosophical Magazine*, 95(28-30), 3305-3327.

Pel, L. (1995). "Moisture transport in porous building materials." Technische Universiteit Eindhoven, Eindhoven, Netherlands.

Roels, S., and Carmeliet, J. (2006). "Analysis of moisture flow in porous materials using microfocus X-ray radiography." *International Journal of Heat and Mass Transfer*, 49(25), 4762-4772.

Rucker-Gramm, P., and Beddoe, R. E. (2010). "Effect of moisture content of concrete on water uptake." *Cement and Concrete Research*, 40(1), 102-108.

Šavija, B. (2014). "Experimental and numerical investigation of chloride ingress in cracked concrete." PhD thesis, Delft University of Technology, Delft, Netherlands.

Šavija, B., Liu, D., Smith, G., Hallam, K. R., Schlangen, E., and Flewitt, P. E. (2016). "Experimentally informed multi-scale modelling of mechanical properties of quasi-brittle nuclear graphite." *Engineering Fracture Mechanics*, 153, 360-377.

Šavija, B., Luković, M., Hosseini, S. A. S., Pacheco, J., and Schlangen, E. (2015). "Corrosion induced cover cracking studied by X-ray computed tomography, nanoindentation, and energy dispersive X-ray spectrometry (EDS)." *Materials and Structures*, 48(7), 2043-2062.

Šavija, B., Luković, M., Pacheco, J., and Schlangen, E. (2013). "Cracking of the concrete cover due to reinforcement corrosion: a two-dimensional lattice model study." *Construction and Building Materials*, 44, 626-638.

Šavija, B., Luković, M., and Schlangen, E. (2014). "Lattice modeling of rapid chloride migration in concrete." *Cement and Concrete Research*, 61, 49-63.

Šavija, B., Luković, M., and Schlangen, E. "Experimental and Numerical Study of Water Uptake in Strained SHCC." *Proc., 10th International Conference on Mechanics and Physics of Creep, Shrinkage, and Durability of Concrete and Concrete Structures*.

Šavija, B., Pacheco, J., and Schlangen, E. (2013). "Lattice modeling of chloride diffusion in sound and cracked concrete." *Cement and Concrete Composites*, 42, 30-40.

Šavija, B., Schlangen, E., Pacheco, J., Millar, S., Eichler, T., and Wilsch, G. (2014). "Chloride ingress in cracked concrete: a laser induced breakdown spectroscopy (LIBS) study." *Journal of Advanced Concrete Technology*, 12(10), 425-442.

Schlangen, E., and Van Mier, J. (1992). "Simple lattice model for numerical simulation of fracture of concrete materials and structures." *Materials and Structures*, 25(9), 534-542.

Van Mier, J. G. (2012). *Concrete fracture: a multiscale approach*, CRC press.

Vasic, S., Smith, I., and Landis, E. (2005). "Finite element techniques and models for wood fracture mechanics." *Wood Science and Technology*, 39(1), 3-17.

Wang, L., and Ueda, T. (2011). "Mesoscale modeling of water penetration into concrete by capillary absorption." *Ocean Engineering*, 38(4), 519-528.

Wang, P., Wittmann, F. H., Zhang, P., Lehmann, E., and Zhao, T. (2014). "Durability and service life of elements made with SHCC under imposed strain." *SHCC3: Proceedings of the 3rd International RILEM Conference on Strain Hardening Cementitious Composites, Dordrecht, The Netherlands*, E. Schlangen, G. Ye, M. Luković, and M. Sierra-Beltran, eds.

Wong, H., Head, M., and Buenfeld, N. (2006). "Pore segmentation of cement-based materials from backscattered electron images." *Cement and Concrete Research*, 36(6), 1083-1090.

Yip, M., Mohle, J., and Bolander, J. (2005). "Automated Modeling of Three-Dimensional Structural Components Using Irregular Lattices." *Computer Aided Civil and Infrastructure Engineering*, 20(6), 393-407.

Yoon, S., Wang, K., Weiss, W. J., and Shah, S. P. (2000). "Interaction between loading, corrosion, and serviceability of reinforced concrete." *ACI Materials Journal*, 97(6), 637-644.

Zhang, P., Wittmann, F., Zhao, T., and Lehmann, E. (2010). "Neutron imaging of water penetration into cracked steel reinforced concrete." *Physica B: Condensed Matter*, 405(7), 1866-1871.

Zhou, J., Qian, S., Beltran, M. G. S., Ye, G., van Breugel, K., and Li, V. C. (2010). "Development of engineered cementitious composites with limestone powder and blast furnace slag." *Materials and Structures*, 43(6), 803-814.